wave functions of high accuracy for the two-electron systems can be found in the form of variationally chosen linear combinations of hydrogenic wave functions of the proper symmetry unless continuum functions are included. This statement follows from the fact that a relatively poor wave function may yield a relatively good energy, or stated in other words, the minor components of a wave function as measured by their contribution to the energy may make up proportionately a much larger part of the wave functions. This result is well-known, and specific examples have been given in earlier papers in the present series.[2,3] As a further illustration, one sees from Table IX that in the superposition of $1s^2$ and $1s2s$ the ratio $c_{1s2s}$ to $c_{1s^2}$ is 0.32 but the ratio of the contributions to the ground state energy of the $1s2s$ configuration and the interaction term between the $1s^2$ and the $1s2s$ to the contribution of the $1s^2$ configuration is 0.13.

In summary, the present work has presented expansions of the various angular components of the three-parameter wave function of Hylleraas for the He I ground state in terms of symmetrized products of hydrogenic wave functions for different values of the parameter, $Z$. The results of these expansions are interpreted in terms of configuration interaction. The changing importance of the different configurations with changing $Z$ is illustrated. In particular, the minimum with respect to $Z$ of the integral over all positive $\epsilon$ of $(c_{1s\epsilon s})^2$ is pointed out. The implications of these results are discussed for attempts to obtain wave functions for both ground and excited states of two-electron systems by the minimum principle from linear combinations of products of hydrogen functions of the proper symmetry.

The authors wish to thank Anita Y. Schwab for help in the computations leading to Tables IV and VI.

PHYSICAL REVIEW VOLUME 96, NUMBER 2 OCTOBER 15, 1954

# Auger Ejection of Electrons from Tungsten by Noble Gas Ions

HOMER D. HAGSTRUM
*Bell Telephone Laboratories, Murray Hill, New Jersey*
(Received June 16, 1954)

Experimental investigation of electron ejection from atomically clean tungsten by singly and multiply charged ions of the noble gases is reported. Total electron yield, $\gamma_i$, and distribution in kinetic energy of the secondary electrons have been measured. Ion energies range from 10 to 1000 ev for singly charged ions. $\gamma_i$ is found in each case to be roughly constant over this interval although the variations observed are significant and can be accounted for by theory. $\gamma_i$ values of 0.293, 0.213, 0.094, 0.047, and 0.018 were obtained for 10 ev $He^+$, $Ne^+$, $Ar^+$, $Kr^+$, and $Xe^+$ ions, respectively. Comparison with theory makes it quite clear that for 10-ev ions essentially all electrons observed are ejected by a process of Auger neutralization in which the interaction of two conduction electrons causes one electron to neutralize the ion in the ground state and the other to be excited into the continuum above the filled band. The observed $\gamma_i$ is determined by the probability that these excited electrons escape from the metal. In the case of $Ne^+$, indications are that as ion energy increases toward 100 ev a two-stage electronic transition process occurs in a small fraction of the encounters. In this process the ion is first resonance neutralized to an excited state and the resulting excited atom is subsequently de-excited in an Auger ejection process. Variation of the electron energy distribution with ion energy has been investigated. Careful measurement for $Ne^{20}$ and $Ne^{22}$ at 200 ev shows $\gamma_i$ to be independent of nuclear mass. Results of $\gamma_i$ and energy distribution measurements for electrons from multiply charged ions up to $Xe^{5+}$ are also reported. A value of *ca* 6.3 ev for the energy of the Fermi level above the ground state in the conduction band in tungsten comes out of this work.

## I. INTRODUCTION

A SERIES of studies of electron ejection from atomically clean metals by ions of the noble gases is extended in this work to tungsten. The singly charged ions of He, Ne, Ar, Kr, and Xe, as well as a number of the multiply charged ions ranging up to $Xe^{5+}$, have been used. Evidence presented indicates the tungsten surface to be atomically clean.

The use of singly charged ions of all the noble gases has proved to be particularly fruitful. Comparison with theory shows that for very slow ions (<10 ev) essentially all the electrons are ejected from tungsten by the process of direct Auger neutralization. Here the role of the incoming ion is to provide a low-lying vacant electronic level (its ground state) for the Auger process. Since the position of this level is determined by the ionization energy of the atom, it is clearly advantageous to study the process for a series of ions.

Of interest is the somewhat anomalous case of $Ne^+$ on tungsten. Here it appears that for ions of energies near 100 ev a fraction (~10 percent) of the ions are resonance neutralized, the excited atoms so formed being subsequently de-excited in an Auger process in which a secondary electron may be ejected. The explanation of the restriction of this possibility to $Ne^+$ and the means of its detection in that case are thought to be particularly convincing of the essential correctness of the theoretical picture.

The detailed interpretation of the results for tungsten is used as illustrative material in the companion paper on theory.[1] Identification of experimental results with theoretical ideas is made here, however. A summary of the basic experimental results which theory is called upon to explain is included in Sec. IX. Experimental apparatus and procedure are dealt with only briefly (Sec. II) inasmuch as these have already been treated in a separate publication.[2] Vacuum conditions, particularly those obtaining with $CO_2$ and acetone on the traps, and the evidence concerning the state of the target surface are discussed in Sec. III. Measurements of total electron yield for singly charged ions and for a pair of isotopic ions are presented in Secs. IV and V, respectively. Energy distribution measurements for slow ions including the dependence on kinetic energy of the incident ion are discussed in Secs. VII and VIII. Results for multiply charged ions are given in Sec. VIII.

No attempt has been made to explain theoretical ideas referred to in this paper. For this reason much of the discussion here presupposes familiarity with the content of the accompanying paper on theory.[1] Notation used is defined as introduced in the text (see also Table I of the accompanying paper on theory[1]).

## II. EXPERIMENTAL APPARATUS AND PROCEDURE

The apparatus used in this investigation is a form of mass spectrometer in which ions produced by electron impact in a gas are mass analyzed and then focussed on the target by electrostatic lenses. The target is a ribbon which can be flashed to high temperature for cleaning. The geometry of the target and surrounding spherical electron collector is such as to make possible quite acceptable retarding potential measurements on electrons leaving the target. This instrument has been discussed extensively as Instrument II in the paper on experimental apparatus and procedure.[2]

Liquid nitrogen (77.4°K) was used on the traps in the studies involving He and Ne. For Ar, Kr, and Xe the traps were cooled with a $CO_2$ and acetone mixture (194.7°K). In the latter case it was found convenient to use gas reservoirs containing mixtures of the noble gases as follows. One reservoir contained He, Ne, and Kr, a second, Ar and Xe. The mixed gases from either of these reservoirs could be independently leaked into the system. These combinations were chosen so as to avoid serious overlapping of singly and multiply charged ions in the mass spectrum. By properly adjusting the electron beam energy it was always possible to find isotopic peaks of a given $m/e$ with no contaminating admixture of an ion from another gas.

Pressure was measured with a Bayard-Alpert type ionization manometer and adsorption rate measurements were used to investigate the state of the target surface. Contact potential between target and electron collector and work function of the target were measured as described elsewhere (see Figs. 20 and 21, respectively, of reference 2).

The use of the heavier noble gas ions in this work necessitated the use of higher magnetic fields in the mass analysis. This brought with it the problem of a higher fringing magnetic field in the neighborhood of the target. The effect of this field on the measured electron energy distributions and the steps taken to reduce the magnetic field intensity inside the electron collector are discussed in Sec. VI.

## III. VACUUM CONDITIONS AND THE STATE OF THE TUNGSTEN SURFACE

Background pressure in the apparatus with liquid nitrogen on the traps was in the range of $2\text{–}4\times10^{-10}$ mm Hg as measured with the ionization manometer ($N_2$ calibration).[3] These conditions were achieved by the "more drastic" evacuation procedure described in the paper on instrumentation and procedure.[2] As is discussed in Sec. VII of the instrumentation paper the actual background pressure must have been in the $10^{-11}$ mm Hg range. The monolayer adsorption time $\Delta t_m$ is seen from Fig. 1 to be of the order of 14 hours. Assuming the same sticking probability and monolayer surface density as for $N_2$ on tungsten one calculates a partial pressure of the adsorbable component in the background gas of about $2\times10^{-11}$ mm Hg.[4]

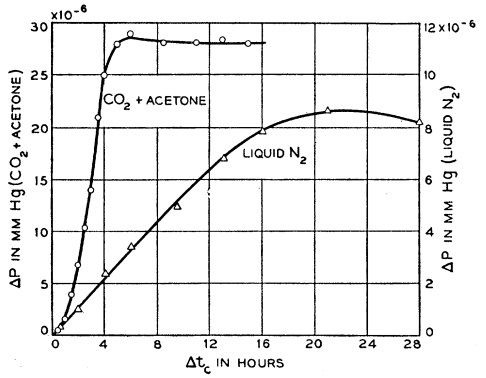


FIG. 1. Curves of pressure rise on target flash $\Delta p$ *vs* cold interval $\Delta t_c$ for background gas (or vapor) in the instrument taken with liquid $N_2$ and with $CO_2$ and acetone cooling on the traps. Pressure readings are those obtained with the ionization gauge calibrated for nitrogen. The monolayer adsorption time, $\Delta t_m$, is the value of $\Delta t_c$ at which the curve departs from the initial linear rise. Some evidence of a maximum in the curve for liquid $N_2$ cooling is to be seen (see reference 9).

[1] H. D. Hagstrum, following paper [Phys. Rev. **96**, 336 (1954)].
[2] H. D. Hagstrum, Rev. Sci. Instr. **24**, 1122 (1953).

[3] The ionization manometer used in the present work had a plate wire of 0.010-in. diameter. Thus a somewhat higher x-ray limit is to be expected with it than with a gauge having a plate wire of smaller diameter.

[4] Use is made of the observation of Becker and Hartman, J. Phys. Chem. **57**, 153 (1953) that a monolayer of $N_2$ forms on tungsten in about one second at $10^{-6}$ mm Hg ($p\Delta t_m \cong 10^{-6}$ mm Hg×sec). These authors give 0.6 as the mean sticking probability

The tungsten target was flashed to 2200°K. This is a temperature sufficiently high to remove oxygen very rapidly[5] and is assumed in this work to be sufficiently high to remove any other adsorbed atoms which may be present. The monolayer adsorption time was found to rise somewhat when He or Ne were admitted indicating admission of adsorbable impurities with these gases. However, the $\Delta t_m$ remained well above 5 hours with liquid $N_2$ on the traps and with the pressure of these noble gases in the target chamber in the range $1\text{–}4\times10^{-7}$ mm Hg.

When the refrigerant on the traps was changed from liquid $N_2$ to the $CO_2$ and acetone mixture, the background pressure reading, with the gauge calibration for $N_2$, rose from the neighborhood of $2\times10^{-10}$ to about $1\times10^{-8}$ mm Hg. Over a period of time the pressure reading was found to vary between $8\times10^{-9}$ and $1.4\times10^{-8}$ mm Hg. Some correlation was found between the observed pressure reading and the amount of $CO_2$ solid in the refrigerant and how well it was mixed. If the observed pressure rise is caused solely by the rise in Hg vapor pressure admitted to the system, the true pressure is obtained from the above readings by multiplying by 0.29.[6]

It seems quite clear that the residual pressure in the system with $CO_2$ and acetone on the traps is to be attributed to mercury vapor. Using the vapor pressure formula for Hg given by Kelley,[7] one calculates the vapor pressure at the sublimation temperature of $CO_2$ to be $2.66\times10^{-9}$ mm Hg. This is in good agreement with the observed pressure range of $2.3\text{–}4.0\times10^{-9}$ mm Hg (gauge reading corrected by the factor 0.29 to the Hg calibration). The variability in the residual pressure reading seems not unreasonable when it is noted that the observed pressure range could be spanned by less than a 4°K temperature change of the bath. Perhaps the only other possible vapor which could be responsible for the residual pressure is that of water. That there must have been very little water vapor present is indicated by the fact that the vapor pressure of $H_2O$ at 194.7°K is *ca* $4\times10^{-4}$ mm Hg.

Attributing the residual pressure with $CO_2$ and acetone on the traps to Hg makes the $\Delta p$ *vs* $\Delta t_c$ curve of Fig. 1 look reasonable. The value of $\Delta p$ at $\Delta t_c > \Delta t_m$ is *ca* $28\times10^{-6}$ mm Hg on the $N_2$ calibration. If this is multiplied by 0.29 one obtains $8.1\times10^{-6}$ mm Hg as the true pressure in agreement with the observed $\Delta p$ for $\Delta t_c > \Delta t_m$ with liquid $N_2$ on the traps. A consistent picture is then obtained if the monolayer surface density of adsorbed atoms or molecules is about the same in the two cases. The vapor pressure of Hg at 77.4°K, calculated from Kelley's formula,[7] comes out to be *ca* $4\times10^{-35}$ mm Hg.

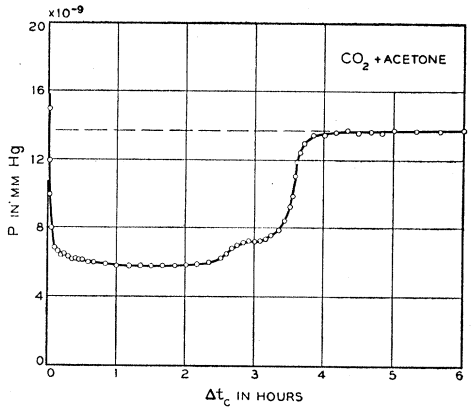


FIG. 2. Curve of pressure, $p$, *vs* cold interval, $\Delta t_c$, with $CO_2$ and acetone cooling on the traps. The background pressure is $13.8\times10^{-9}$ mm Hg if the calibration for $N_2$ gas is used or $4\times10^{-9}$ mm Hg if the calibration for mercury vapor is used. The kink in the curve between 2.6 and 2.9 hours is perhaps not significant. Refrigerant on the traps was renewed at 2.9 hours. Note that the monolayer is formed in about 3.5 hours.

The data of Fig. 1 show a monolayer adsorption time of about 4 hours with $CO_2$ and acetone on the traps. From this an estimate of the sticking probability of Hg on tungsten may be obtained. Since the pressure was about $3\times10^{-9}$ mm Hg (using the Hg calibration) $p\Delta t_m \simeq 4.3\times10^{-5}$ mm Hg×sec. This is about 50 times the $p\Delta t_m$ value of $N_2$ on tungsten.[4] Hence the sticking probability of Hg on tungsten is about 0.02 times that of $N_2$ on tungsten or about 0.01. From this it is also clear that the partial pressure of adsorbable impurity having a sticking probability near that of nitrogen could certainly be no more than 0.02 times the observed pressure. This is perhaps another evidence that the pressure observed is to be attributed predominantly to Hg. Finally, baking of the apparatus and the traps followed by cooling directly with the $CO_2$ and acetone mixture produced no change in the observed background pressure.

A $p$ *vs* $\Delta t_c$ curve with $CO_2$ and acetone on the traps is shown in Fig. 2. It indicates general agreement with the $\Delta p$ *vs* $\Delta t_c$ curve of Fig. 1.

Admission of either the He-Ne-Kr or the Ar-Xe mixture produced an increase in the initial slope of the $\Delta p$ *vs* $\Delta t_c$ curve (Fig. 1) of about two. This would indicate a corresponding decrease in $\Delta t_m$ due to admission of adsorbable impurities or some small adsorption of the heavier noble gases themselves. Under the least favorable conditions $\Delta t_m$ is still of the order of two hours or more. One may thus have confidence that the tungsten surface is atomically clean to within a

---

of $N_2$ on tungsten. Other work (private communication) shows the observed sticking probability to vary in the range 0.2 to 0.6 from sample to sample presumably depending on crystal orientation on the surface. Figure 16 of reference 2 indicates that for $N_2$ on molybdenum $p\Delta t_m \sim 1.8\times10^{-6}$ mm Hg×sec.

[5] I. Langmuir and D. S. Villars, J. Am. Chem. Soc. **53**, 495 (1931), report on oxygen film to be removed from tungsten at 2070°K at a rate such that half disappeared in 20 seconds. I. Langmuir, J. Am. Chem. Soc. **35**, 105 (1913), found $O_2$ to affect the thermionic emission from tungsten at $T<2200$°K.

[6] S. Dushman and A. H. Young, Phys. Rev. **68**, 278 (1945).

[7] K. K. Kelley, Bulletin 383, U. S. Bureau of Mines, Washington, 1935 (unpublished), p. 69 gives $\Delta F^\circ = -RT\ln p = 15\,455 + 0.92T\log T + 0.003T^2 - 30.06T$ for the vapor pressure of Hg in bars above solid Hg at the temperature $T$°K.

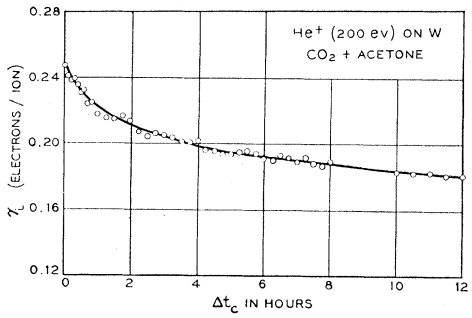


FIG. 3. Total electron yield, $\gamma_i$, *versus* target cold interval, $\Delta t_c$, for $He^+$ ions of 200-ev energy incident on tungsten with $CO_2$ and acetone cooling on the traps.

few percent for measurements made within minutes of a target flash. All data reported here meet this requirement.

A further evidence of the cleanliness of the tungsten surface comes from the observation of total secondary yield with time after a target flash. Such data for $He^+$ ions of 200 ev, obtained from the He-Ne-Kr mixture with $CO_2$ and acetone on the traps, are plotted in Fig. 3. The rate of change of $\gamma_i$ with time as a gas layer forms on the target surface is clearly slow enough to permit measurements under clean conditions.

The target is made of tungsten ribbon 0.015 in. thick and 7 mm wide. On removal from the experimental tube it appeared to be thermally etched. Back reflection Laue patterns showed the surface to consist of crystals of 0.05 to 0.3 mm in size. The x-ray goniometer showed no high degree of crystal orientation, the 100 plane making angles up to $\pm 30°$ with the plane of the surface.

## IV. $\gamma_i$ FOR SINGLY CHARGED IONS

The data for $\gamma_i$ of singly charged ions in the kinetic energy range 10 to 1000 ev are plotted in Fig. 4. These data were taken with the electron collector five volts positive relative to the target to insure collection of all ejected electrons. Collector voltages considerably higher than five volts were found to increase noticeably the loss of slow electrons through the entrance aperture.

The data on $\gamma_i$ indicate a number of features relating to the magnitude of $\gamma_i$ and its variation with incident ion energy. Perhaps the most striking feature is the small dependence of $\gamma_i$ on ion kinetic energy. This is a basic evidence that the ejection process is an Auger process in which ion kinetic energy plays only a very secondary role.

A second interesting feature is the magnitude of $\gamma_i$. For no ion is it greater than 0.3, and for 10-ev ions it is seen to decrease steadily as one passes through the sequence from the lighter to the heavier ions. It is now clear that the Auger processes are so probable that the magnitude of $\gamma_i$ is determined by the probability of the excited electron escaping from the metal rather than by the probability that the process occur while the ion is near the surface. The decrease in $\gamma_i$ from $He^+$ to $Xe^+$ is, of course, the result of decreasing ionization energy. The depth in the metal from which an electron can be ejected by Auger neutralization is approximately $E_i/2$. The ground state of the conduction band in tungsten lies some 10.9 ev below the zero vacuum level. Thus, whereas for He and Ne all, or essentially all, electrons excited in the Auger process have enough energy to leave the metal if properly directed, in Ar, Kr, and Xe only electrons raised from the top approximately 50, 40, and 25 percent of the filled portion of the band, respectively, have any chance of leaving the metal.

Although essentially independent of ion energy the $\gamma_i$ data of Fig. 4 show some energy dependences which are thought to be significant and for which reasons can be given. These are largely the results of broadening of the electron energy distribution as the ion is neutralized closer to the metal at higher incident energy. This can be shown to account both for the initial drop in $\gamma_i$ of $He^+$ and the rise in $\gamma_i$ of $Ar^+$, $Kr^+$, and $Xe^+$. The rise in $\gamma_i(He^+)$ at higher energies (above 400 ev) is probably the result of electron ejection by a process other than Auger ejection, perhaps of the type discussed by Ploch[8] in which bound electrons are released from surface atoms. One should expect the probability of such ejection to increase with the ion's incident velocity. It should appear at lowest energy in the case of the lightest and hence fastest ion ($He^+$ and $He^{++}$). Further evidence on this point is obtained from the

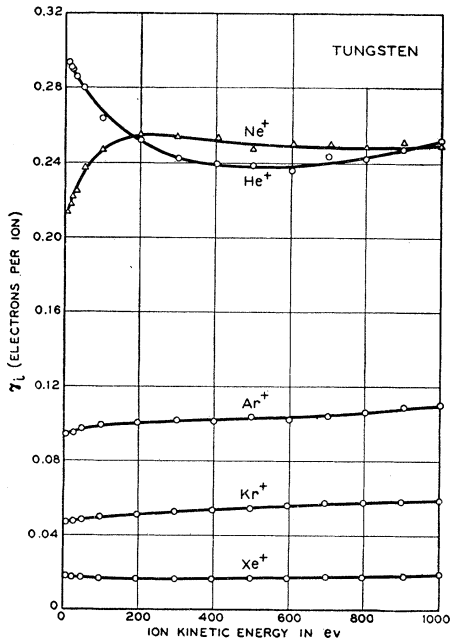


FIG. 4. Total electron yield, $\gamma_i$, *vs* ion kinetic energy for singly charged ions of the noble gases on atomically clean tungsten.

[8] W. Ploch, Z. Physik **130**, 174 (1951); see also M. E. Gurtovoy, J. Exptl. Theoret. Phys. (U.S.S.R.) **10**, 483 (1940).

electron energy distributions (Sec. VI). The anomalous behavior of $\gamma_i(Ne^+)$ is to be attributed to the increase in the proportion of the two-stage ejection process with increasing ion velocity. It is interesting to note that $\gamma_i(He^+)$ on molybdenum exhibited the same dependence on $E_k(He^+)$ as is reported here.[9]

The variation of $\gamma_i(He^+)$ with ion energy below 200 ev is very sensitive to surface contamination. $\gamma_i$ at low ion energy is larger the cleaner the surface. It was found that during the course of the measurements $\gamma_i$ values thought to be characteristic of an atomically clean surface slowly rose. At 10 ev, for example, this rise in $\gamma_i(He^+)$ was from 0.26 to 0.29. As indicated in the instrumentation paper[2] it is difficult even under the best conditions to reduce the residual adsorbed gas to less than about 1 percent of a monolayer.

The value of $\gamma_i$ at ion energies a few times thermal energy is of interest in gaseous electronics. It has been possible to estimate $\gamma_i$ at energies below those actually used in the experiment from the theory of the variation of $\gamma_i$ with incident ion energy (Sec. XV of the accompanying paper).[1]

## V. $\gamma_i$ FOR ISOTOPIC IONS

$\gamma_i$ has been measured carefully for $Ne^+$ ions of $m/e=20$ and 22 at 200-ev ion energy. 35 readings of $\gamma_i$ for each ion were made alternately. The current from the source was adjusted to give amplifier readings for each ion on the same shunt and the same meter deflection to within 5 percent. The target was flashed every third reading so as to treat measurements for the two ions alike. The average $\gamma_i$ for both sets of

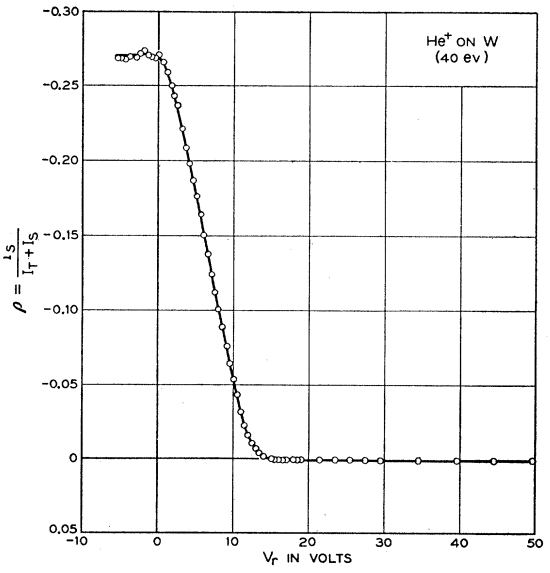


FIG. 5. Typical retarding potential data from which an electron energy distribution is obtained by the method described in the text. $V_r$ is the voltage between target and electron collector corrected for contact potential.

[9] H. D. Hagstrum, Phys. Rev. **89**, 244 (1953).

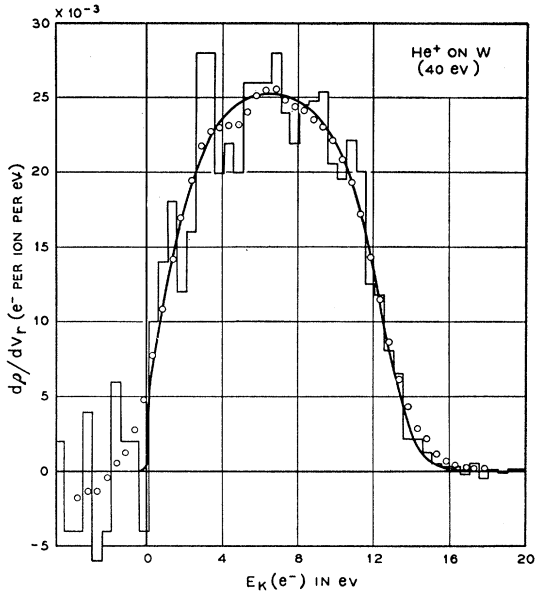


FIG. 6. Plots of $\Delta\rho/\Delta V_r$ and a smoothed $d\rho/dV_r$ curve from the data of Fig. 5. The points are $d\rho/dV_r$ values obtained from the smoothing formula given in the text.

35 readings came out to be 0.2561 with a standard deviation in each case very close to 0.0014.

Thus $\gamma_i$ is found not to depend on the isotope used. This is clearly what one would expect for these Auger processes. The result is of some interest, however, in view of the results of Ploch[8] on the mass dependence of the electron yield for isotopic ions, in particular $Ne^+$ on beryllium and platinum. The present results do not necessarily contradict Ploch's since he used faster ions and surfaces which were most likely not atomically clean. Both of these conditions favor kinetic ejection. The slope of his $\gamma_i$ *vs* ion energy curves even at 1 kev do not agree with the present work but look much like results the author has obtained with contaminated surfaces.

## VI. ELECTRON ENERGY DISTRIBUTIONS FOR SLOW IONS

Electron energy distributions are measured in this work by means of retarding potentials. Currents to the electron collector $I_S$ and to the target $I_T$ are measured as functions of $V_{ST}$, the voltage between target and collector. The ratio of currents $\rho=I_S/(I_T+I_S)$ is obtained as a function of retarding potential $V_r$ which is $V_{ST}$ corrected for contact potential (see Fig. 5). Contact potential between target and collector was measured several times during the course of the experiment and found to lie in the range 0.3 to 0.4 v (target positive). This did not change on replacing liquid $N_2$ with $CO_2$ and acetone on the traps. These measurements and the characteristics of the $\rho$ *vs* $V_r$ curve are discussed in the paper on instrumentation and procedure.[2]

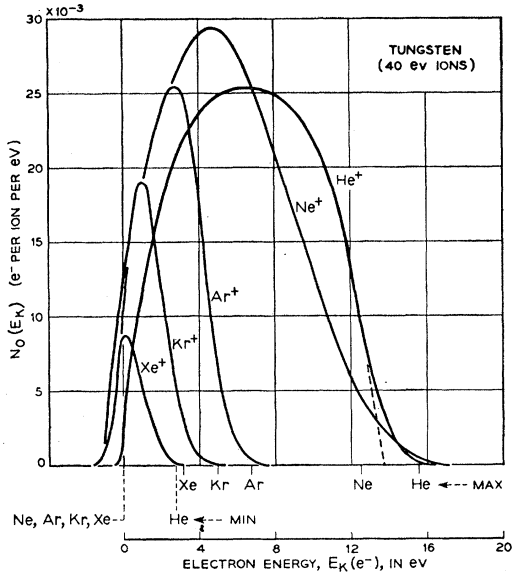


FIG. 7. Energy distribution functions $N_0(E_k)$ for electrons ejected from atomically clean tungsten by singly charged noble gas ions of 40-ev incident kinetic energy. The maximum and minimum energies indicated on the abscissa scale are the values $E_i-2\varphi$ and $E_i-2\epsilon_0$ or zero, respectively. These are the maxima and minima to be expected on the simple theory in which energy level shifts in the atom near the metal surface and broadening of the distributions are not taken into account.

In the present work the energy distribution $N_0(E_k)=d\rho/dV_r$ has been obtained from the retarding potential data in the following way. First $\Delta\rho/\Delta V_r$ is plotted from the $\rho$ *vs* $V_r$ data of Fig. 5 as shown by the stepped curve in Fig. 6. Smoothed values of the slope $d\rho/dV_r$ are also calculated from a smoothing formula, suggested to the author by Kaplan[10] which we shall discuss presently. The points plotted in Fig. 6 are those obtained from this formula. The $N_0(E_k)$ distribution is obtained by drawing a smooth curve through the stepped function being guided by the points obtained from the smoothing formula. The smoothing formula departs quite radically from the true curve wherever $d^2\rho/dV_r^2$ is large as is seen near the low- and high-energy limits of the curve in Fig. 6. In other regions, however, the smoothed points are helpful in drawing the final curve.

Kaplan suggested a smoothing formula based on the following considerations. If the data were precise the slope at a point, designated $(n+\frac{1}{2})$, which lies halfway between the points at $(V_r)_n$ and $(V_r)_{n+1}$ is $(d\rho/dV_r)_{n+\frac{1}{2}}=(\rho_{n+1}-\rho_n)/\Delta V_r$, where $\Delta V_r=(V_r)_{n+1}-(V_r)_n$. If the data are not precise, the slope at $(n+\frac{1}{2})$ of a straight line fitted to the data by least squares is $(d\rho/dV_r)_{n+\frac{1}{2}}=2(\cdots-3\rho_{n-1}-\rho_n+\rho_{n+1}+3\rho_{n+2}+\cdots)/\Delta V_r(\cdots 3^2+1^2+1^2+3^2+\cdots)$. Whereas the first formula puts all the weight on the data points adjacent to the point $(n+\frac{1}{2})$, the second formula weights most heavily data points which are most distant from the point $(n+\frac{1}{2})$. The compromise suggested by Kaplan weights equally all data points used. Eight data points are smoothed by the formula:

$$\left(\frac{d\rho}{dV_r}\right)_{4\frac{1}{2}}=\frac{\rho_1+\rho_2+\rho_3+\rho_4-\rho_5-\rho_6-\rho_7-\rho_8}{16\Delta V_r}.$$

The procedure followed here is thought to be more accurate than that of measuring the slope of a smoothed $\rho$ *vs* $V_r$ plot as was done in earlier work.[9]

Energy distributions, $N_0(E_k)=d\rho/dV_r$, obtained in the manner just described for electrons ejected by $He^+$, $Ne^+$, $Ar^+$, $Kr^+$, and $Xe^+$, are plotted in Fig. 7. Note that the curves extend more or less to the left of the zero axis. This is an experimental effect resulting from the presence in the target-collector region of a small, uncompensated magnetic field fringing from the magnet of the *m/e* analyzer. For $He^+$ this fringing field is negligible. For the heavier ions, on the other hand, it becomes appreciable. Most of the fringing field has been balanced out by a field applied by a magnet which straddles the tube in the region of the target.[2] This bucking field is adjusted to optimum by observing a value of $\rho$ on the steep side of the $\rho$ *vs* $V_r$ characteristic (Fig. 5) as a function of auxiliary magnet current. One finds the field which maximizes this $\rho$ value. Such data for $Xe^+$ are plotted in Fig. 8. The optimum current for Xe is seen to be 3 ma corresponding to a target magnetic field of some 12 gauss. Since the fringing field at the target is *ca* 45 gauss at the field used for $Xe^+$, it is evident that the presence of the target magnet itself shunts the fringing field in the target region. Similar settings of the target magnet current were determined for each analyzer magnetic

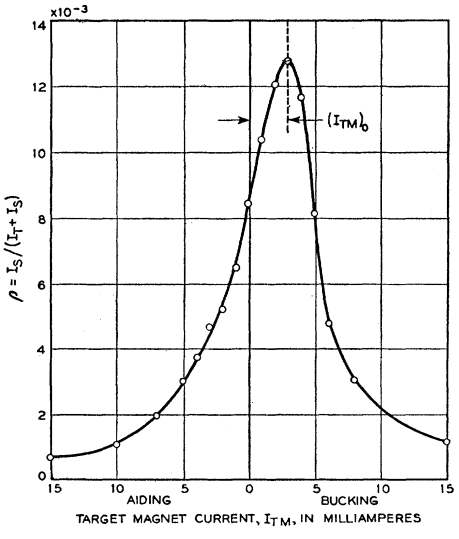


FIG. 8. The value of $\rho[=I_S/(I_T+I_S)]$ at a point on the steep slope of the $\rho$ *vs* $V_r$ characteristic plotted as a function of current through the coils of a magnet which straddles the tube in the region of the target.

[10] The author is also indebted to R. W. Hamming for a helpful discussion on data smoothing.

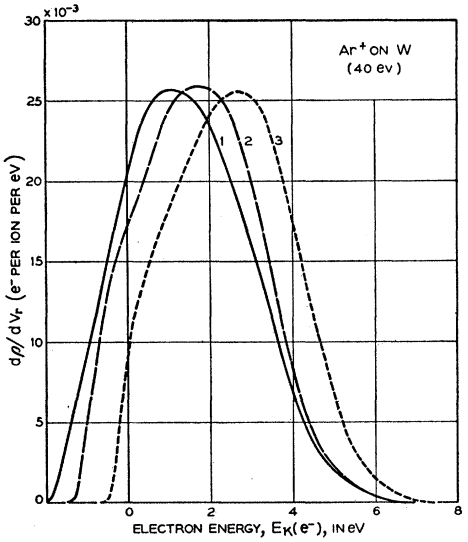


FIG. 9. Illustration of the effect of fringing magnetic field on the determination of the electron energy distribution function for electrons ejected by $Ar^+$. Curve 1: fringe field uncompensated, analyzer magnetic field of 1840 gauss; curve 2: fringe field uncompensated, analyzer field 1350 gauss; curve 3: fringe field compensated, analyzer field 1840 gauss. Note that in the compensated case (curve 3) some extension of the curve to negative $E_k(e^-)$ indicates incomplete compensation over the entire volume of the electron collector.

field used. All data presented in this paper were taken with the fringing field compensated for in this manner. The fact that the $N_0(E_k)$ curves of Fig. 7 do extend to negative $E_k(e^-)$ in spite of this procedure indicates that the fringe field is not balanced out uniformly over the volume of the 4 cm diameter collector sphere. Since $rB=3.4$ cm-gauss for a 1 ev electron it is clear that the residual field must be reduced considerably below 1 gauss if its effect is to be unobservable. The effect on an energy distribution function of failure to compensate for fringing field is shown in Fig. 9. The figure is explained in the caption. Analyzer

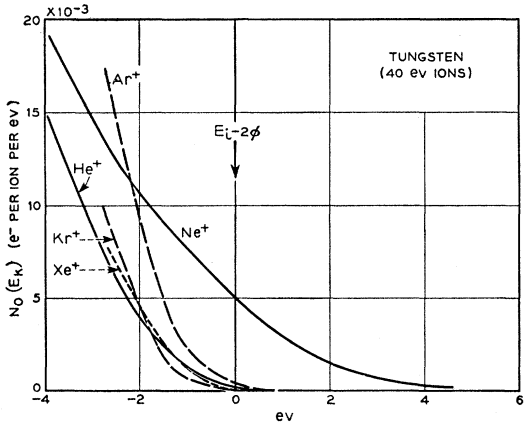


FIG. 10. A plot of the high energy tails of the distributions of Fig. 7 in which the curves have been shifted along the abscissa axis, so that the values $E_i-2\varphi$ for all distributions coincide.

magnetic fields normally used are: $He^+$, 580; $Ne^+$, 1300; $Ar^+$, 1840; $Kr^+$, 2670; $Xe^+$, 3200 gauss. With no compensation or magnetic shielding, fringe fields at the target position would be *ca* 1.5 percent of these values.

We now discuss briefly the distribution function data. In the first place two important data come directly from the retarding potential curve, $\rho$ *vs* $V_r$ (Fig. 5). One is $\gamma_i=\rho$ at $V_r<0$, already discussed in Sections IV and V. The other is the very low positive value of $\rho$ at $V_r>E_k(e^-)_{\max}$, the maximum energy of ejected secondary electrons. This indicates very small reflection of slow ions as ions or as metastable atoms. $\rho$ at $V_r>E_k(e^-)_{\max}$ is found to increase with increasing ion energy indicating greater reflection at higher incident energies.[11]

The forms of the energy distribution functions of Fig. 7 are of particular theoretical interest in as much as theory predicts such functions with which the experi-

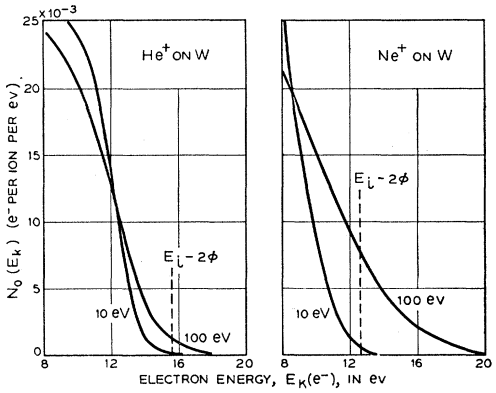


FIG. 11. Plots of tails of $N_0(E_k)$ distributions for $He^+$ and $Ne^+$ ions at 10- and 100-ev incident kinetic energies. Note agreement with the limit $E_i-2\varphi$ in each case at 10 ev. Note also that $Ne^+$ displays a much greater violation of the $E_i-2\varphi$ limit than does $He^+$ as ion energy is increased.

mentally determined ones may be compared. Furthermore, the form is found to be sensitive to the state of the target surface.[12] Of more specific interest, however, is the form of the distribution function near the minimum and maximum energy. Evidence is to be seen in Fig. 7 of a marked depletion of slow electrons in the distribution for $He^+$ compared to the $Ne^+$ and $Ar^+$ distributions. Investigation of the reasons behind this observation leads to a value (*ca* 6.3 ev) for the width $\epsilon_F$ of the filled portion of the conduction band in tungsten.[1]

The experimental data concerning the forms of the distributions near their energy maxima are perhaps more clearly shown in Fig. 10 than in Fig. 7. In Fig.

[11] These evidences of reflection of ions as ions and as metastable atoms have been studied further and will be reported in a separate publication now in preparation.

[12] Work is in progress on the effect on Auger ejection of adsorption of common gases on the target surface. A preliminary report is in print: H. D. Hagstrum, Phys. Rev. 89, 338 (1953).

10 the high-energy tails of the distributions for 40-ev ions are plotted to an energy scale on which $E_i-2\varphi$ for all ions coincide. This makes it clearly evident that for $He^+$, $Ar^+$, $Kr^+$, and $Xe^+$ the maximum energy is quite close to the $E_i-2\varphi$ limit but that for $Ne^+$ it is not. This state of affairs can be shown to result from the fact that for $He^+$, $Ar^+$, $Kr^+$, and $Xe^+$ only Auger neutralization occurs, whereas at 40 ev in some 10 percent of the $Ne^+$ encounters the two-stage process of resonance neutralization and Auger de-excitation results. To demonstrate the validity of this conclusion it is necessary to show (1) that for Auger neutralization an energy limit at or below $E_i-2\varphi$ is expected, (2) that for Auger de-excitation this limit may be exceeded, and (3) that resonance neutralization can occur at an atomically clean tungsten surface only for $Ne^+$. This

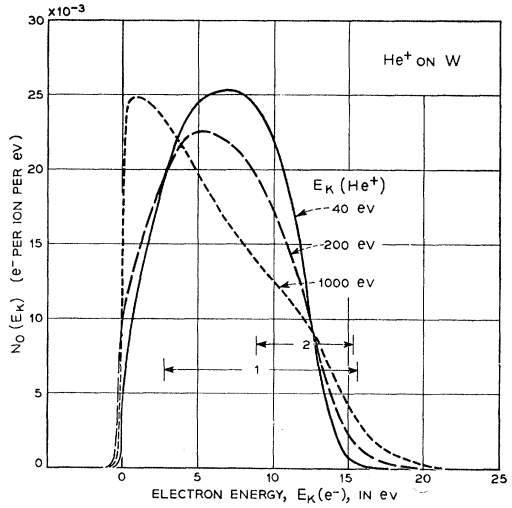


FIG. 12. Energy distributions of electrons ejected by $He^+$ ions of 40-, 200-, and 1200-ev incident kinetic energy. The energy intervals labeled 1 and 2 here and in Fig. 13 are those predicted for Auger neutralization and de-excitation, respectively, if energy level shifts near the metal and broadening of the distribution are neglected.

demonstration is undertaken in the paper on theory.[1] The theory indicates further that the rise in $\gamma_i(Ne^+)$ at low energies (see Fig. 4 and Sec VII) results from an increase in the fraction of two-stage processes with increasing ion energy and that for 10-ev ions the fraction of two-stage processes is essentially zero. If this is the case we expect no violation of the $E_i-2\varphi$ limit even in the case of $Ne^+$ at 10 ev. That this is indeed found to be the case is seen in Fig. 11. Here the high-energy tails of the $N_0(E_k)$ distributions for $He^+$ and $Ne^+$ are plotted for 10- and 100-ev ions. For 10-ev ions in each case the distribution limit agrees well with the $E_i-2\varphi$ limit. For $He^+$ at 100 ev this limit is exceeded by an amount which is readily attributable to the broadening of the distribution due to the causes discussed in Sec. XII of the theory paper.[1] For $Ne^+$ at 100 ev, on the other hand, a very much larger tail is evident which

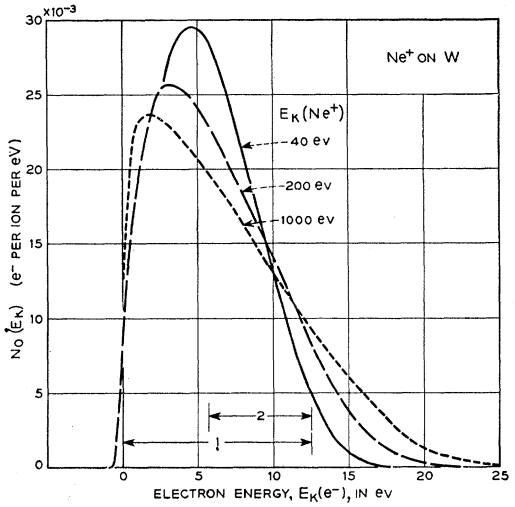


FIG. 13. Energy distributions of electrons ejected by 40-, 200-, and 1000-ev $Ne^+$ ions. See caption of Fig. 12 for explanation of the intervals labeled 1 and 2.

can only result from electrons ejected in the Auger de-excitation process.

## VII. VARIATION OF ELECTRON ENERGY DISTRIBUTION WITH ION KINETIC ENERGY

Electron energy distributions have been determined for each of the singly charged ions at incident ion energies of 40, 200, and 1000 ev. Results for $He^+$, $Ne^+$, and $Kr^+$ are plotted in Figs. 12, 13, and 14, respectively. These three cases are representative of distinguishable variations with initial energy to be expected theoretically.

For all cases we expect and observe an extension of the distribution to higher electron energies at higher ion energies. This is the result of the greater broadening of the distribution for processes occurring closer to the

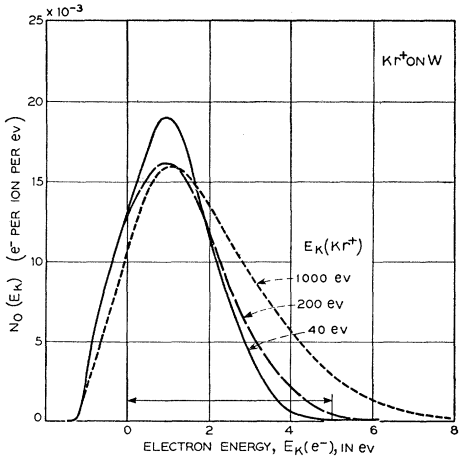


FIG. 14. Energy distributions of electrons ejected by 40-, 200-, and 1000-ev $Kr^+$ ions. The changes observed for $Kr^+$ are representative of those observed for $Ar^+$ and $Xe^+$. The energy interval indicated corresponds to that labeled 1 in Figs. 12 and 13 (see caption of Fig. 12).

metal as is the case when the ion approaches more rapidly. For $Ne^+$ the admixture of electrons from Auger de-excitation is seen to cause a much greater violation of the $E_i-2\varphi$ limit at ion energies above 10 ev than is observed for the other ions. The agreement with the limit at 10 ev and its explanation is thought to be good experimental confirmation of the theory. For both $He^+$ and $Ne^+$ we observe a relative increase in the number of slow electrons, as the ion energy is increased. The effect of broadening only is observed for $Kr^+$. This difference is traceable to the fact that for $He^+$ and $Ne^+$ all, for $Kr^+$ only a fraction, of the internal electrons excited in the Auger process have sufficient energy to surmount the surface barrier if properly directed. How each of the characteristics mentioned

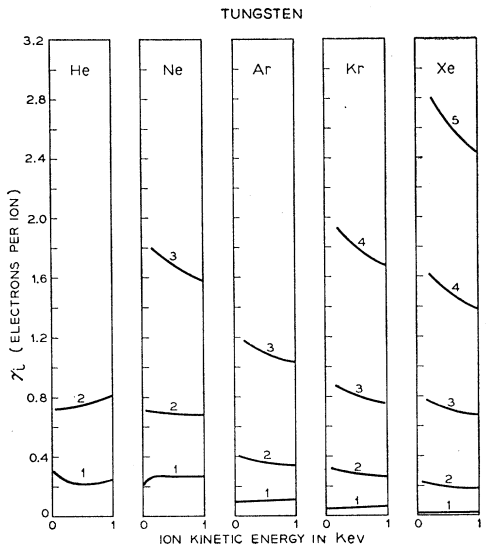


FIG. 15. Total yield *vs* ion kinetic energy for singly and multiply charged ions of the noble gases incident upon atomically clean tungsten. The charge of the ion is indicated at each curve.

here arises is discussed in detail in the companion paper on theory.[1]

$He^+$ ions of 1000-ev energy are observed to eject a relatively larger number of slow electrons [$E_k(e^-)<5$ ev] for which theory can give no account. It is suggested that these are electrons ejected in non-Auger processes. Such have been postulated (Sec. IV) to account for the slow rise in $\gamma_i(He^+)$ above 400 ev where theory predicts a steady decrease. The failure to observe a disproportionate number of slow electrons for $Ne^+$ is then to be correlated with the observation that $\gamma_i(Ne^+)$ does not rise at higher ion energies. It should be pointed out that the distribution $N_0(E_k)$ plotted as $d\rho/dV_r$ should be corrected for the term $dR/dV_r$ [see Eq. (6) of reference 2] which is appreciable at 1000 ev. Removal of this term would in no way affect the conclusions stated above.

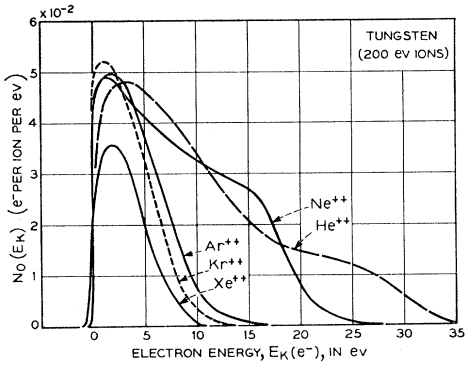


FIG. 16. Energy distributions of electrons ejected from tungsten by doubly charged ions of the noble gases. In this case $N_0(E_k)=2d\rho/dV_r$. Ion energy in each case is 200 ev.

## VIII. RESULTS FOR MULTIPLY CHARGED IONS

The results obtained in this work for multiply charged ions are to be found in Figs. 15 through 20. They include measurements of total yield as a function of ion energy (Fig. 15) and of electron energy distribution. Distribution for all doubly and triply charged ions are plotted together in Figs. 16 and 17, respectively. Although included in Figs. 16 and 17 the distributions for the Ne ions are plotted together in Fig. 18 to illustrate the particularly interesting evidence of "inclusion" of the distribution for a given ion in the distribution of the ion of next higher charge. Data for Kr and Xe ions not plotted in Figs. 16 and 17 are to be found in Figs. 19 and 20, respectively.

There are some five experimental conclusions having theoretical implications which come out of this work. These are:

1. $\gamma_i$ is found to increase with ionic charge and hence total ionization energy. This is thought to be the result of the neutralization of multiply charged ions near the metal surface in a series of stages at each one of which an electron is excited inside the metal. Subject to some qualification this means more electrons but not faster ones as the charge of the ion increases (see item 3 below). A more detailed look at this situation is obtained if the ratios of electron yield and total ioniza-

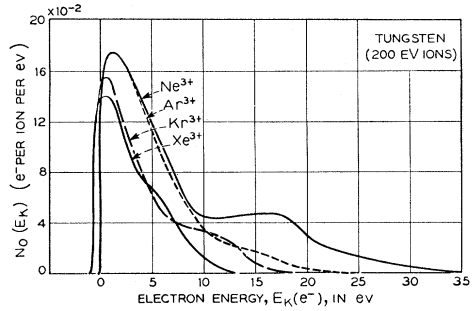


FIG. 17. Energy distributions of electrons ejected from tungsten by triply charged ions of the noble gases of 200-ev energy [$N_0(E_k)=3d\rho/dV_r$].

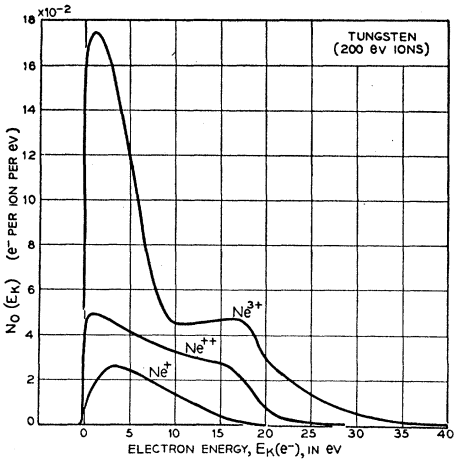


FIG. 18. Energy distributions of electrons ejected from tungsten by 200-ev neon ions $[N_0(E_k)=zd\rho/dV_r$ where $z$=ionic charge].

tion energy for ions which differ by one unit of charge are compared (Table I). Here it is seen that for He and Ne and for the more highly charged ions of Ar, Kr, and Xe reasonable agreement between these ratios prevails. This is not true for the less highly charged ions of the heavier gases (lower left-hand corner of Table I). If one assumes that multiply charged ions are neutralized in a series of approximately isoenergetic steps one can understand the main features of Table I as follows. For the lighter atoms and the more highly charged heavier ions the energy released per step in the neutralization process is sufficient to excite all or nearly all electrons above the surface barrier. The escape probability then cancels out of the ratio of electron yields which should then be approximately equal to the ratio of total energies available. For the ions $Ar^+$, $Kr^+$, and $Xe^+$, on the other hand only a fraction of the excited electrons have enough energy to escape. Since this fraction can increase markedly for

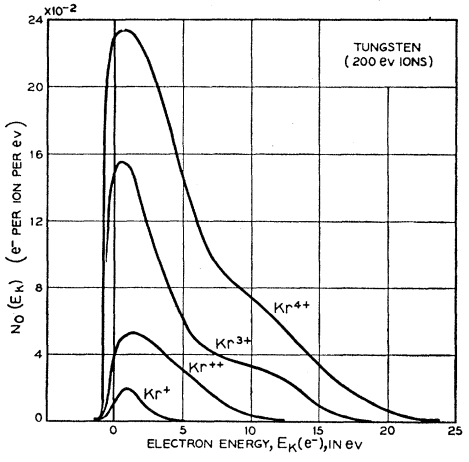


FIG. 19. Energy distributions of electrons ejected from tungsten by 200-ev krypton ions.

the doubly charged ion it is reasonable that the ratio of $\gamma_i$ values exceed the ratio of $E_i$ values. This effect is greatest for Xe which has the lowest ionization energy.

2. $\gamma_i$ for each of the multiply charged ions except $He^{++}$ is found to drop with increasing ion energy. This is taken to result from the broadening of the component energy distributions as the steps of neutralization occur closer to the metal. The explanation is thus the same as that of the drop in $\gamma_i(He^+)$ with increasing ion energy. Each step in the cascade neutralization process thus produces a distribution in energy of excited electrons inside the metal which lies above the zero vacuum level and for which broadening can be shown to reduce the chance of escape. The exception of $He^{++}$ remains unexplained. It is probable that for $He^{++}$ as for $He^+$ some electrons are released from surface atoms. This process should become more probable with increasing ion energy. It is interesting to note that of the ions used this ion is the only one which is a bare nucleus without any surrounding electrons.

3. Although faster electrons are produced with more highly charged ions, by and large the mean energy of the ejected electrons is relatively independent of ionic charge. This observation is in agreement with, and is indeed good evidence for, the conclusion that neutralization occurs predominantly in a series of steps.

TABLE I. Ratios of electron yield ($\gamma_i$) and total ionization energy ($E_i$) for ions which differ by one unit of charge.

| Atom | 2+/1+ $\gamma_i$ | 2+/1+ $E_i$ | 3+/2+ $\gamma_i$ | 3+/2+ $E_i$ | 4+/3+ $\gamma_i$ | 4+/3+ $E_i$ | 5+/4+ $\gamma_i$ | 5+/4+ $E_i$ |
|---|---|---|---|---|---|---|---|---|
| He | 2.6 | 3.2 | | | | | | |
| Ne | 3.1 | 2.9 | 2.5 | 2.0 | | | | |
| Ar | 4.3 | 2.8 | 3.0 | 2.0 | | | | |
| Kr | 6.8 | 2.8 | 2.9 | 2.0 | 2.2 | 1.7 | | |
| Xe | 12.0 | 2.8 | 3.5 | 1.9 | 2.0 | 1.8 | 1.8 | 1.5 |

4. The maximum in the $N_0(E_k)$ curve appears to be a function of ionic charge but is essentially independent of mass (ionization energy) of the ion. Thus the maxima of the $N_0(E_k)$ curves for doubly charged ions (Fig. 16) are near $5\times10^{-2}$ electron per ion per ev and for triply charged ions (Fig. 17) near $16\times10^{-2}$ electron per ion per ev. These figures may be compared with the approximately $2.5\times10^{-2}$ electron per ion per ev value for singly charged ions (Fig. 7). The falling off toward the heavier ions is thought to be the result of the lower ionization energy and the consequent inability of all excited electrons to escape if properly directed. This effect is less apparent the higher the ionic charge, as is reasonable. The increase in the maximum values of $N_0(E_k)$ noted here is really only another manifestation of the step-by-step neutralization process. It may perhaps be taken as evidence of greater similarity in the neutralization schemes than the ratios of total yield alone would require.

5. There is evidence in the data of the "inclusion"

of the energy distribution for a given ion in that for the ion of next higher charge (see Fig. 18). This is further evidence pointing to the stepwise neutralization through ions of lower charge to the ground state of the neutral atom.

## IX. SUMMARY OF EXPERIMENTAL RESULTS FOR SINGLY CHARGED IONS

In conclusion a listing is given of the experimental results for singly charged ions. The list is restricted to the results for singly charged ions inasmuch as a similar listing of results for multiply charged ions has already been given in Sec. VIII.

1. The total electron yield, $\gamma_i$, depends in a relatively minor way on ion kinetic energy.
2. $\gamma_i$ is uniformly less than 0.3.
3. $\gamma_i$ for the slowest ions decreases steadily with decreasing ionization energy.
4. The smaller variations of $\gamma_i$ with ion energy are:
   a. The drop in $\gamma_i(He^+)$ at ion energy up to 400 ev
   b. The rise in $\gamma_i(He^+)$ above 400 ev,
   c. The rise in $\gamma_i(Ne^+)$ up to 100 ev,
   d. The general rise in $\gamma_i$ for $Ar^+$, $Kr^+$, and $Xe^+$ with ion energy.
5. $\gamma_i$ is independent of ionic mass.
6. Very few ions are reflected as ions or as metastable atoms.
7. The maxima in electron energy are approximately $E_i-2\varphi$ for the $He^+$, $Ar^+$, $Kr^+$, and $Xe^+$.
8. The electron energy maximum for $Ne^+$ appreciably exceeds $E_i-2\varphi$ for ions of kinetic energy greater than 10 ev but agrees with this limit at 10 ev.
9. In all cases the high-energy tails of the electron energy distribution become more pronounced with increasing ion energy.
10. For $He^+$ fewer low-energy electrons are observed than for $Ne^+$ and $Ar^+$.
11. For $He^+$ and $Ne^+$ increase in ion energy results in a relative increase in the number of slow electrons.

It is interesting to note that all of these observations with two exceptions can be accounted for in terms of the processes of Auger neutralization, resonance neutralization, and Auger de-excitation. The rise in $\gamma_i(He^+)$ above 400 ev and the increase in the number of slow electrons with increasing $He^+$ energy appear to be anomalous. As has been suggested it is reasonable that these effects arise from a small amount of ejection (non-Auger) by the ion when it is very close to the metal or has penetrated into the lattice.*

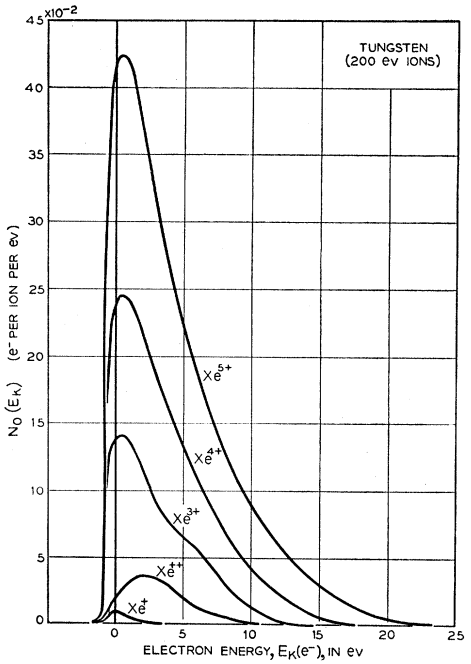


FIG. 20. Energy distributions of electrons ejected from tungsten by 200-ev xenon ions.

The author wishes to acknowledge with thanks the work of C. D'Amico, who took the data which are published here.

* *Note added in proof.*—Very recently it has been found that metastably excited singly charged ions are produced in Ar, Kr, and Xe if the bombarding electrons are fast enough. Such ions are detectable only by the fact that their ability to eject electrons from a metal is greater than that of unexcited singly charged ions. Work to be published later shows that the values of $\gamma_i$ reported here for $Ar^+$, $Kr^+$, and $Xe^+$ are approximately 5 percent, 10 percent, and 30 percent larger, respectively, than they should be for ions all of which are unexcited.